Journal of Coordination Chemistry

ISSN: 0095-8972 (Print) 1029-0389 (Online) Journal homepage: http://www.tandfonline.com/loi/gcoo20

Architectural diversity of six coordination compounds based on (S)-(+)-mandelic acid and different N-donor auxiliary ligands: syntheses, structures, and luminescent properties

Wei-Ying Guo, Meng-Li Li, Ya-Jing Shi, Hui-Hua Song & Hai-Tao Yu

To cite this article: Wei-Ying Guo, Meng-Li Li, Ya-Jing Shi, Hui-Hua Song & Hai-Tao Yu (2015) Architectural diversity of six coordination compounds based on (S)-(+)-mandelic acid and different N-donor auxiliary ligands: syntheses, structures, and luminescent properties, Journal of Coordination Chemistry, 68:23, 4224-4241, DOI: 10.1080/00958972.2015.1100300

To link to this article: http://dx.doi.org/10.1080/00958972.2015.1100300

Journal of Coordination Chemistry, 2015
Vol. 68, No. 23, 4224–4241, http://dx.doi.org/10.1080/00958972.2015.1100300

Architectural diversity of six coordination compounds based on (*S*)-(+)-mandelic acid and different N-donor auxiliary ligands: syntheses, structures, and luminescent properties

WEI-YING GUO, MENG-LI LI, YA-JING SHI, HUI-HUA SONG* and HAI-TAO YU

College of Chemistry and Material Sciences, Hebei Normal University, Shijiazhuang, China

(*Received 18 January 2015; accepted 17 August 2015*)

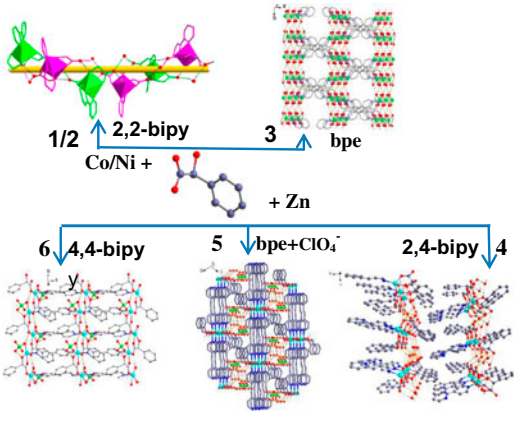

Six transition metal coordination compounds with H_2mand and different N-donor ligands, [Co(Hmand)$_2$(2,2′-bipy)]·H_2O (**1**), [Ni(Hmand)$_2$(2,2′-bipy)]·H_2O (**2**), [Ni(Hmand)$_2$(bpe)] (**3**), [Zn(Hmand)$_2$(2,4′-bipy)(H_2O)]·$2H_2O$ (**4**), [Zn(Hmand)(bpe)(H_2O)]$_n$[(ClO_4)]$_n$·nH_2O (**5**), and [Zn(Hmand)(4,4′-bipy)(H_2O)]$_n$[(ClO_4)]$_n$ (**6**), were synthesized under different conditions (H_2mand = (*S*)-(+)-mandelic acid, bpe = 1,2-di(4-pyridyl)ethane, 4,4′-bipy = 4,4′-bipyridine, 2,4′-bipy = 2,4′-bipyridine, 2,2′-bipy = 2,2′-bipyridine). Their structures were determined by single-crystal X-ray diffraction analysis and further characterized by elemental analysis, infrared spectra, thermogravimetric analysis, powder X-ray diffraction, and circular dichroism. Compounds **1** and **2** are isostructural (0-D structures), which are extended to supramolecular 1-D chains by hydrogen bonding. Compound **3** exhibits 1-D straight chain structures, which are further linked via hydrogen bond interactions to generate a 3-D supramolecular architecture. Compound **4** displays a discrete molecular unit. Neighboring units are further linked by hydrogen bonds and π–π interactions to form a 3-D supramolecular architecture. Compound **5** displays a 2-D undulated network, further extended into a 3-D supramolecular architecture through hydrogen bond interactions. Compound **6** possesses a 2-D sheet structure. Auxiliary ligands and counteranions play an important role in the formation of final frameworks, and the hydrogen-bonding interactions and π–π stacking interactions contributed to the formation of the diverse supramolecular architectures. Compounds **1**, **2**, **4**, **5,** and **6** crystallize in chiral space groups, with the circular dichroism spectra exhibiting positive cotton effects. Furthermore, the luminescent properties

*Corresponding author. Email: songhuihua@mail.hebtu.edu.cn

of **4**–**6** have been examined in the solid state at room temperature, and the different crystal structures influence emission spectra significantly.

Keywords: Coordination compounds; (*S*)-(+)-Mandelic acid; Crystal structure; Circular dichroism; Luminescent properties

1. Introduction

Chirality has been of great importance in chemistry, biochemistry, and materials science [1–3]. Recently, chiral coordination polymers have received extensive attention for diverse topologies, intriguing structure, and potential applications in enantioselective synthesis, asymmetric catalysis, nonlinear optical materials, luminescence, and magnetic materials [4–11]. Generally, introduction of chiral templates or chiral ligands to direct the homochiral crystallization of intrinsically chiral coordination polymers has proved to be a very effective method. However, the synthesis of chiral coordination polymers with desirable structures and properties is still arduous [12–15]. A possible reason may be that crystallization is a very complicated process, in which subtle changes such as additional ligands, metal, pH, counteranion, and reaction temperature, make it difficult to predict effects on final compositions and structures [16–20]. Among various chiral organic ligands, α-hydroxycarboxylic acids, exhibiting a variety of coordination abilities and the tendency to form architectures with multidimensional frameworks, are appealing ligands for building chiral coordination compounds [21]. Mandelic acid, as an α-hydroxydicarboxylic acid, which consists of phenyl, hydroxyl, and carboxyl groups, possesses ability to synthesize chiral coordination polymers. Owing to these functional groups, the mandelic acid ligand creates many possibilities for formation of inter- and intra-molecular interactions through aromatic interactions and hydrogen bonds to stabilize the structure of chiral coordination polymers [22–25]. A number of chiral network materials of mandelic acid ligand have been reported. Yogo *et al*. reported the discovery of a 1-D chiral coordination polymer, [Cu-($C_6H_5CH(OH)COO$)(μ-$C_6H_5CH(OH)COO$)], which showed piezoelectric properties and second harmonic generation activity [22], while Fedin *et al*. succeeded in preparing a series of porous coordination polymers with mandelic acid [26], and Luneau *et al*. synthesized 1-D chiral molecular-magnets $\{M^{II}(L/D\text{-mand})(4\text{-MePy})_3\}_n \cdot n(ClO_4)$ ($M = Co^{II}$ and Ni^{II}) [27]. However, there are very few reports which discuss the structures of different N-donor auxiliary ligands around metal centers.

Our group has been committed to exploitation of chiral coordination compounds based on chiral ligands. We have synthesized a series of chiral complexes and made a systematic investigation into how external conditions such as temperature, auxiliary ligands, metal, etc. influence the structures and properties [28–31]. Pursuing our work in this area, we selected (*S*)-(+)-mandelic acid as ligand and a series of N-donor ligands to synthesize chiral coordination compounds. Herein, we report six coordination compounds, $[Co(Hmand)_2(2,2'\text{-bipy})]\cdot H_2O$ (**1**), $[Ni(Hmand)_2(2,2'\text{-bipy})]\cdot H_2O$ (**2**), $[Ni(Hmand)_2(bpe)]$ (**3**), $[Zn(Hmand)_2(2,4'\text{-bipy})(H_2O)]\cdot 2H_2O$ (**4**), $[Zn(Hmand)(bpe)(H_2O)]_n[(ClO_4)]_n \cdot nH_2O$ (**5**), and $[Zn(Hmand)(4,4'\text{-bipy})(H_2O)]_n[(ClO_4)]_n$ (**6**) (H_2mand = (*S*)-(+)-mandelic acid, bpe = 1,2-di(4-pyridyl)ethane, 4,4′-bipy = 4,4′-bipyridine, 2,4′-bipy = 2,4′-bipyridine, 2,2′-bipy = 2,2′-bipyridine), which are characterized by X-ray crystallography, elemental analysis, IR

spectra, thermal stability, powder X-ray diffraction (PXRD), and circular dichroism (CD). Furthermore, the solid-state luminescent properties of **4**–**6** were studied.

2. Experimental

2.1. *Materials and methods*

All reagents and solvents for syntheses were purchased from commercial sources and were used as received. Elemental analyses (C, H, and N) were performed on an Elemental Vario EL elemental analyser. Infrared (IR) spectra were (KBr pellets) measured on a FTIR-8900 spectrometer from 4000 to 400 cm^{-1}. Thermogravimetric analyses (TGA) were carried out on a simultaneous STA 449F3/TENSOR 27 thermal analyzer under nitrogen with a heating rate of 10 °C min^{-1} from room temperature to 800 °C. The PXRD patterns were checked at room temperature. The solid-state CD spectra were recorded on a JASCOJ-810 spectropolarimeter with KCl pellets. Fluorescence spectra were recorded on a Hitachi F-4500 luminescence spectrometer.

2.2. *Synthesis*

2.2.1. Synthesis of [Co(Hmand)$_2$(2,2′-bipy)]·H$_2$O (1). $Co(Ac)_2{\cdot}4H_2O$ (0.0498 g, 0.2 mmol), H_2mand (0.0608 g, 0.4 mmol), and 2,2′-bipy (0.0624 g, 0.4 mmol) were mixed in a solution containing ethanol (25.0 mL). The solution was adjusted to pH 5.4 with addition of a dilute aqueous 2 mol/L NaOH solution. The mixture was stirred for 5 min at room temperature and filtered. The filtrate was left to stand at room temperature for about two weeks to deposit orange diamond-shaped crystals of **1**. Yield: ~55% (based on Co). Anal. Calcd for $C_{26}H_{24}N_2O_7Co$ (%). C, 58.55; H, 4.46; N, 5.25. Found: C, 58.32; H, 4.51; N, 5.23. IR (KBr, cm^{-1}) *v*: 3524(b), 1578(s), 1493(w), 1475(w), 1443(m), 1395(m), 1340(w), 1283(m), 1250(w), 1196(w), 1154(w), 1080(w), 1053(m), 1024(m), 957(w), 789(w), 767 (m), 743(m), 798(m), 652(w), 606(m), 552(m), 509(w), 459(w).

2.2.2. Synthesis of [Ni(Hmand)$_2$(2,2′-bipy)]·H$_2$O (2). The mixture of H_2mand (0.0304 g, 0.2 mmol) and 2,2′-bipy (0.0312 g, 0.2 mmol) was stirred into a 15-mL aqueous solution, which was heated in a water bath at 60 °C for about 10 min. Then, the freshly prepared Ni $(OH)_2$ was added until a small amount of precipitate was formed. The resulting solution was stirred for 20 min, filtered off, and allowed to stand for two weeks. The blue diamond-shaped crystals obtained were suitable for X-ray analysis. Yield: ~53% (based on Ni). Anal. Calcd for $C_{26}H_{24}N_2NiO_7$ (%). C, 58.35; H, 4.52; N, 5.23. Found: C, 58.49; H, 4.56; N, 5.41. IR (KBr, cm^{-1}) *v*: 3451(b), 1578(s), 1494(w), 1475(w), 1445(m), 1398(m), 1342(w), 1285(m), 1196(w), 1154(w), 1081(w), 1055(m), 1029(m), 958(w), 766(m), 743(m), 700(m), 655(w), 608(m), 554(m), 419(w).

2.2.3. Synthesis of [Ni(Hmand)$_2$(bpe)] (3). The mixture of H_2mand (0.0304 g, 0.2 mmol) and bpe (0.0368 g, 0.2 mmol) was stirred into a solution containing H_2O (7 mL) and methanol (3 mL). Then, the freshly prepared $Ni(OH)_2$ was added until a small amount of precipitate was formed. The mixture was homogenized for 30 min at room temperature,

transferred to a sealed 23-mL Teflon-lined stainless reactor, and heated at 140 °C for four - days under autogenous pressure. Afterward, the reaction mixture was allowed to cool to room temperature and filtered. The blue diamond-shaped crystals were separated from the mother liquor by slow evaporation at room temperature after 10 days. Yield: ~33% (based on Ni). Anal. Calcd for $C_{28}H_{26}N_2NiO_6$ (%). C, 61.68; H, 4.81; N, 5.14. Found: C, 60.98; H, 4.68; N, 5.12. IR (KBr, cm^{-1}) *v*: 3436(b), 3058(m), 2477(b), 1612(w), 1581(s), 1498 (w), 1450(m), 1378(w), 1345(w), 1288(w), 1246(w), 1224(w), 1197(w), 1089(m), 1060(m), 1019(w), 944(w), 829(s), 815(w), 797(m), 740(s), 700(m), 673(w), 610(w), 551(s), 495(w), 466(w).

2.2.4. Synthesis of $[Zn(Hmand)_2(2,4'\text{-bipy})(H_2O)]\cdot 2H_2O$ (4). $Zn(ClO_4)_2\cdot 6H_2O$ (0.0372 g, 0.1 mmol), H_2mand (0.0304 g, 0.2 mmol), and 2,4′-bipy (0.0312 g, 0.2 mmol) were mixed in a solution containing H_2O (6 mL) and ethanol (6 mL). The mixture was placed in a 23-mL Teflon-lined stainless reactor after adjusting to pH = 4.5 with the addition of a dilute aqueous 1 mol/L NaOH solution, which was then heated to 120 °C for six days. Afterward, the reaction mixture was allowed to cool to room temperature and filtered. The filtrate was left to stand at room temperature for about one week to deposit colorless block-shaped crystals of **4**. Yield: ~58% (based on Zn). Anal. Calcd for $C_{26}H_{28}N_2O_9Zn$ (%). C, 54.04; H, 4.81; N, 4.81. Found: C, 54.03; H, 4.88; N, 4.84. IR (KBr, cm^{-1}) *v*: 3312(b), 1585(s), 1499 (w), 1466(m), 1435(s), 1389(s), 1331(w), 1279(m), 1223(w), 1180(w), 1163(w), 1084(w), 1065(m), 1040(m), 1003(w), 991(w), 951(w), 870(w), 777(m), 700(m), 657(w), 570(w), 497(w), 455(w).

2.2.5. Synthesis of $[Zn(Hmand)(bpe)(H_2O)]_n[(ClO_4)]_n\cdot nH_2O$ (5). Compound **5** was synthesized in a procedure similar to that for **4**, except that bpe was used instead of 2,4′-bipy. The colorless rod-shaped transparent crystals of **5**, suitable for X-ray analysis, were obtained by filtration, washed with deionized water, and dried in air. Yield: ~50% (based on Zn). Anal. Calcd for $C_{20}H_{22}ClN_2O_9Zn$ (%): C, 45.27; H, 4.23; N, 5.22. Found: C, 45.25; H, 4.25; N, 5.28. IR (KBr, cm^{-1}) *v*: 3421(b), 1616(s), 1583(s), 1506(w), 1429(m), 1383(w), 1338(w), 1271(w), 1226(w), 1143(m), 1119(m), 1090(m), 1053(m), 1030(w), 837(w), 825 (w), 786(w), 752(w), 698(m), 626(w), 594(m), 545(w).

2.2.6. Synthesis of $[Zn(Hmand)(4,4'\text{-bipy})(H_2O)]_n[(ClO_4)]_n$ (6). This compound was synthesized in a procedure analogous to that of **4** except that 4,4′-bipy was used instead of 2,4′-bipy. The colorless flake-shaped crystals of **6**, suitable for X-ray analysis, were obtained by filtration. Yield: ~56% (based on Zn). Anal. Calcd for $C_{18}H_{17}ClN_2O_8Zn$ (%): C, 44.59; H, 3.53; N, 5.77. Found: C, 44.10; H, 3.48; N, 5.71. IR (KBr, cm^{-1}) *v*: 3308(b), 1579(s), 1491(w), 1452(w), 1412(m), 1373(w), 1346(w), 1273(w), 1223(m), 1198(w), 1115 (s), 1047(s), 1026(m), 963(w), 926(w), 814(m), 767(m), 729(w), 710(m), 635(m), 550(w), 473(w).

2.3. *X-ray crystal structure determination*

Suitable single crystals for **1**–**6** were selected for single-crystal X-ray diffraction analyses. Crystallographic data were collected at 173 K on a Bruker SMART-CCD diffractometer with graphite-monochromated Mo-Kα radiation (λ = 0.71073 Å). All structures were solved

Table 1. Crystal data and structure refinements for **1–6**.

Compound	**1**	**2**	**3**	**4**	**5**	**6**
Empirical formula	$C_{26}H_{24}CoN_2O_7$	$C_{26}H_{24}N_2NiO_7$	$C_{28}H_{26}N_2NiO_6$	$C_{26}H_{28}N_2O_9Zn$	$C_{20}H_{22}ClN_2O_9Zn$	$C_{18}H_{17}ClN_2O_8Zn$
Formula weight	535.40	535.18	545.22	577.87	535.22	490.16
Temperature (K)	99.97(14)	298(2)	298(2)	100.00(2)	100.00(2)	100.00(2)
Wavelength (Å)	0.71073	0.71073	0.71073	0.71073	0.71073	0.71073
Crystal system	Hexagonal	Hexagonal	Monoclinic	Monoclinic	Monoclinic	Monoclinic
Space group	*P*6(1)22	*P*6(1)22	*C*2/c	*P*2(1)	*P*2(1)	*P*2(1)
a (Å)	11.611(2)	11.6963(8)	25.329(3)	5.75690(10)	11.6092(11)	10.5257(8)
b (Å)	11.611(2)	11.6963(8)	9.9179(12)	28.3754(10)	8.3984(6)	8.3259(4)
c (Å)	31.196(4)	31.276(4)	10.6507(13)	7.6552(2)	12.7066(10)	11.3867(7)
α (°)	90	90	90	90.00	90	90
β (°)	90	90	107.331(2)	91.991(3)	113.018(10)	108.727(7)
γ (°)	120	120	90	90.00	90	90
V (Å^3)	3642.4(10)	3705.4(6)	2554.0(5)	1249.76(6)	1140.24(16)	945.05(10)
Z	6	6	4	2	2	2
Dc (g cm^{-3})	1.459	1.439	1.418	1.536	1.549	1.722
μ (mm^{-1})	0.756	0.834	0.805	1.042	1.222	1.493
F(000)	1650	1668	1136	600	548	500
Reflections collected	10,233	19,593	6571	7420	4762	4094
R_{int}	0.0810	0.0797	0.0176	0.0289	0.0339	0.0300
Data/restraints/parameters	2260/0/164	2302/24/164	2387/12/224	4244/1/344	3162/1/301	3341/1/268
Goodness-of-fit	1.168	1.136	1.076	1.047	1.023	1.041
R_1[a],wR_2[b][$I > 2\sigma(I)$][a]	0.0996, 0.1979	0.0605, 0.1303	0.0266, 0.0720	0.0271, 0.0593	0.0452, 0.0981	0.0395, 0.0756
R_1[a],wR_2[b] (all data)	0.1075, 0.2023	0.0700, 0.1344	0.0292, 0.0739	0.0282, 0.0601	0.0553, 0.1069	0.0454, 0.0798

Table 2. Selected bond lengths (Å) and angles (°) for **1–6**.

1					
Co(1)–O(2)	2.088(5)	O(2)–Co(1)–O(3)	76.56(19)	O(3)–Co(1)–N(1)#1	93.6(4)
Co(1)–O(2)#1	2.088(5)	O(2)#1–Co(1)–O(3)	93.8(2)	O(3)#1–Co(1)–N(1)#1	161.1(3)
Co(1)–O(3)	2.110(6)	O(2)–Co(1)–O(3)#1	93.8(2)	O(2)–Co(1)–N(1)	89.1(3)
Co(1)–O(3)#1	2.110(6)	O(2)#1–Co(1)–O(3)#1	76.6(2)	O(2)#1–Co(1)–N(1)	102.6(3)
Co(1)–N(1)#1	2.110(9)	O(3)–Co(1)–O(3)#1	99.5(4)	O(3)–Co(1)–N(1)	161.1(3)
Co(1)–N(1)	2.110(9)	O(2)–Co(1)–N(1)#1	102.6(3)	O(3)#1–Co(1)–N(1)	93.6(4)
O(2)–Co(1)–O(2)#1	165.2(3)	O(2)#1–Co(1)–N(1)#1	89.1(3)	N(1)#1–Co(1)–N(1)	77.4(7)
2					
N(1)–Ni(1)	2.060(5)	O(2)#1–Ni(1)–N(1)	90.85(14)	N(1)–Ni(1)–O(1)	92.57(18)
Ni(1)–O(2)#1	2.050(3)	O(2)–Ni(1)–N(1)	99.55(14)	N(1)#1–Ni(1)–O(1)	164.77(15)
Ni(1)–O(2)	2.050(3)	O(2)#1–Ni(1)–N(1)#1	99.55(14)	O(2)#1–Ni(1)–O(1)#1	77.49(11)
Ni(1)–N(1)#1	2.060(5)	O(2)–Ni(1)–N(1)#1	90.85(14)	O(2)–Ni(1)–O(1)#1	93.56(12)
Ni(1)–O(1)	2.072(3)	N(1)–Ni(1)–N(1)#1	79.6(3)	N(1)–Ni(1)–O(1)#1	164.77(15)
Ni(1)–O(1)#1	2.072(3)	O(2)#1–Ni(1)–O(1)	93.56(12)	N(1)#1–Ni(1)–O(1)#1	92.57(18)
O(2)#1–Ni(1)–O(2)	166.48(18)	O(2)–Ni(1)–O(1)	77.49(11)	O(1)–Ni(1)–O(1)#1	97.84(18)
3					
N(1)–Ni(1)	2.1343(13)	O(1)–Ni(1)–O(3)#2	99.43(4)	O(3)#2–Ni(1)–N(1)#2	89.24(5)
Ni(1)–O(1)	2.0103(10)	O(1)#2–Ni(1)–O(3)#2	80.57(4)	O(3)–Ni(1)–N(1)#2	90.76(5)
Ni(1)–O(1)#2	2.0103(10)	O(1)–Ni(1)–O(3)	80.57(4)	O(1)–Ni(1)–N(1)	90.33(5)
Ni(1)–O(3)#2	2.0624(10)	O(1)#2–Ni(1)–O(3)	99.43(4)	O(1)#2–Ni(1)–N(1)	89.67(5)
Ni(1)–O(3)	2.0624(10)	O(3)#2–Ni(1)–O(3)	180.0	O(3)#2–Ni(1)–N(1)	90.76(5)
Ni(1)–N(1)#2	2.1343(13)	O(1)–Ni(1)–N(1)#2	89.67(5)	O(3)–Ni(1)–N(1)	89.24(5)
O(1)–Ni(1)–O(1)#2	180.0	O(1)#2–Ni(1)–N(1)#2	90.33(5)	N(1)#2–Ni(1)–N(1)	180.0
4					
N(1)–Zn(1)	2.119(2)	O(2)–Zn(1)–O(6)	162.02(7)	O(6)–Zn(1)–N(1)	93.92(8)
O(2)–Zn(1)	2.0184(18)	O(7)–Zn(1)–O(6)	92.43(6)	O(4)–Zn(1)–N(1)	91.16(8)
O(3)–Zn(1)	2.1248(17)	O(2)–Zn(1)–O(4)	92.83(7)	O(2)–Zn(1)–O(3)	78.41(7)
O(4)–Zn(1)	2.1158(15)	O(7)–Zn(1)–O(4)	168.09(6)	O(7)–Zn(1)–O(3)	89.61(8)
O(6)–Zn(1)	2.1087(18)	O(6)–Zn(1)–O(4)	75.67(6)	O(6)–Zn(1)–O(3)	87.72(7)
O(7)–Zn(1)	2.0649(14)	O(2)–Zn(1)–N(1)	100.19(8)	O(4)–Zn(1)–O(3)	90.28(8)
O(2)–Zn(1)–O(7)	98.81(7)	O(7)–Zn(1)–N(1)	89.25(9)	N(1)–Zn(1)–O(3)	178.04(8)
5					
N(1)–Zn(1)	2.099(4)	N(1)–Zn(1)–O(2)	91.80(18)	O(2)–Zn(1)–O(3)#4	77.7(2)
O(1)–Zn(1)	2.274(4)	N(2)#3–Zn(1)–O(2)	89.50(18)	O(4)–Zn(1)–O(3)#4	125.6(2)
O(2)–Zn(1)	2.124(5)	N(1)–Zn(1)–O(4)	88.52(17)	N(1)–Zn(1)–O(1)	86.78(15)
O(4)–Zn(1)	2.151(4)	N(2)#3–Zn(1)–O(4)	88.84(17)	N(2)#3–Zn(1)–O(1)	90.13(16)
Zn(1)–N(2)#3	2.113(4)	O(2)–Zn(1)–O(4)	156.75(15)	O(2)–Zn(1)–O(1)	72.05(15)
Zn(1)–O(3)#4	2.164(3)	N(1)–Zn(1)–O(3)#4	90.61(14)	O(4)–Zn(1)–O(1)	84.76(16)
N(1)–Zn(1)–N(2)#3	176.11(17)	N(2)#3–Zn(1)–O(3)#4	93.26(14)	O(3)#4–Zn(1)–O(1)	149.5(2)
6					
N(1)–Zn(1)	2.131(3)	O(2)–Zn(1)–N(2)#3	94.59(14)	N(2)#3–Zn(1)–O(1)#4	90.98(11)
N(2)–Zn(1)#1	2.135(3)	N(1)–Zn(1)–N(2)#3	175.11(19)	O(8)–Zn(1)–O(1)#4	126.16(13)
O(1)–Zn(1)#2	2.169(3)	O(2)–Zn(1)–O(8)	157.41(11)	O(2)–Zn(1)–O(3)	73.02(11)
O(2)–Zn(1)	2.098(3)	N(1)–Zn(1)–O(8)	89.11(14)	N(1)–Zn(1)–O(3)	95.08(13)
O(3)–Zn(1)	2.228(3)	N(2)#3–Zn(1)–O(8)	86.35(14)	N(2)#3–Zn(1)–O(3)	86.30(12)
Zn(1)–N(2)#3	2.135(3)	O(2)–Zn(1)–O(1)#4	76.42(13)	O(8)–Zn(1)–O(3)	84.54(13)
Zn(1)–O(1)#4	2.169(3)	N(1)–Zn(1)–O(1)#4	90.23(11)	O(1)#4–Zn(1)–O(3)	148.98(12)
O(2)–Zn(1)–N(1)	90.30(15)				

Notes: Symmetry codes for **1**: #1 x, $x-y$, $-z+1/6$; for **2**: #1 x, $x-y+2$, $-z+1/6$; for **3**: #1 $-x+1$, $-y$, $-z+2$; #2 $-x+1/2$, $-y+1/2$, $-z+2$; for **5**: #1 $x+1$, y, $z+1$; #2 $-x$, $y+1/2$, $-z$; #3 $x-1$, y, $z-1$; #4 $-x$, $y-1/2$, $-z$; for **6**: #1 x, y, $z+1$; #2 $-x+2$, $y-1/2$, $-z$; #3 x, y, $z-1$; #4 $-x+2$, $y+1/2$, $-z$.

through direct methods using the program SHELXTL-97 and refined using SHELXL-97. All non-hydrogen atoms were refined anisotropically by full-matrix least-squares on F^2 using SHELXL-97. The hydrogens were included at their calculated positions. Carbons from bpe ligands were disordered in **3**. Further crystallographic data and experimental details for structural analyses of **1**–**6** are summarized in table 1. The selected bond lengths and angles of **1**–**6** are given in table 2.

3. Results and discussion

3.1. *Structural descriptions of 1–6*

3.1.1. Structure of Co(Hmand)$_2$(2,2′-bipy)·H$_2$O (1). Single-crystal X-ray diffraction analysis indicates that **1** and **2** are isomorphic and crystallize in the same hexagonal space group $P6_122$, as 0-D structures. Therefore, **1** is employed as a representative structure to be described. Co^{2+}, two $Hmand^-$ anions, one 2,2′-bipyridine, and one lattice water are in the asymmetric unit. As shown in figure 1(a), each Co^{2+} is six-coordinate by four oxygens (O2, O3, $O2^{\#1}$, $O3^{\#1}$) from two $Hmand^-$ anions and two nitrogens (N1, $N1^{\#1}$) from one 2,2′-bipyridine ligand. The O3, $O3^{\#1}$, N1, and $N1^{\#1}$ atoms constitute the equatorial plane and O2, $O2^{\#1}$ occupy apical positions. The Co–O bond lengths range from 2.088(5) to 2.110(6) Å and the Co–N bond length is 2.110(9) Å.

$Hmand^-$ is a monoanionic O,O′-bidentate ligand that chelates Co^{2+} through the carboxylic and hydroxyl oxygens to form a five-membered chelate ring (scheme 1(a)). 2,2′-Bipyridine adopts a chelating bidentate mode (scheme 1(c)). There are two kinds of hydrogen-bonding motifs (listed in table 3). In the first motif, water molecules and uncoordinated carboxylic oxygens of $Hmand^-$ (O4–H4···$O1^{\#2}$ = 2.880(9)) are involved in forming a pair of supramolecular helical chains. In the second motif, two supramolecular helical chains are connected via hydrogen bonding between an uncoordinated carboxylato oxygen of $Hmand^-$ in one chain and the coordinated hydroxyl oxygen of $Hmand^-$ (O3–H3···$O1^{\#3}$)

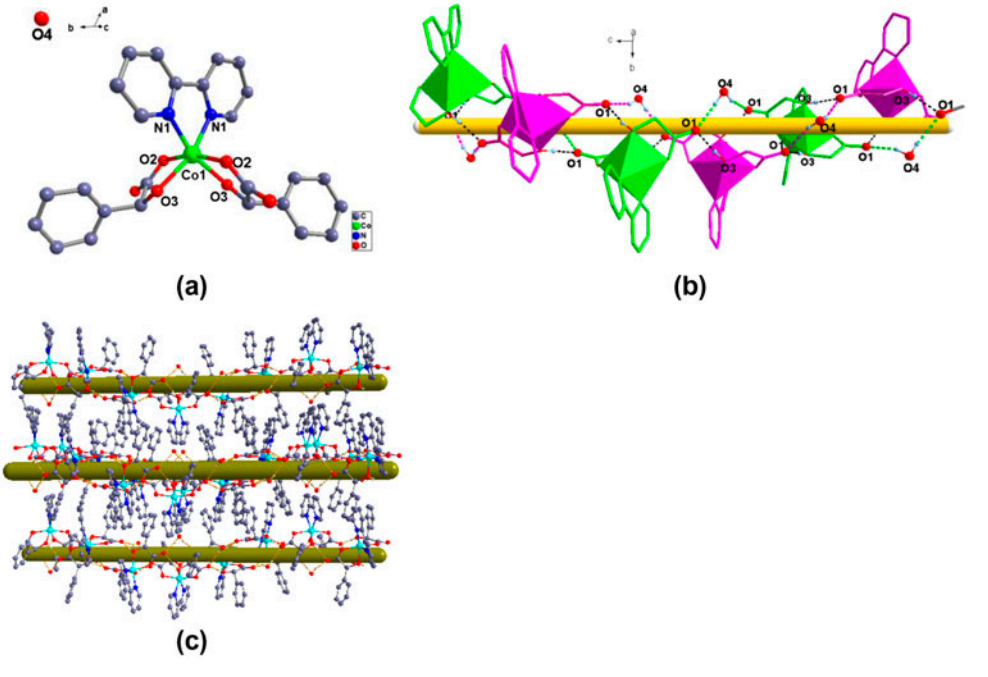

Figure 1. X-ray crystal structure of **1**. (a) X-ray crystal structure of **1**. The coordination environment of Co(II). Hydrogens have been omitted for clarity. (b) Two kinds of hydrogen-bonding motifs of **1**. (Benzene rings of mand-anions and hydrogens have been omitted for clarity.). (c) Representation of the 1-D supramolecular network connected through hydrogen bonds of **1**.

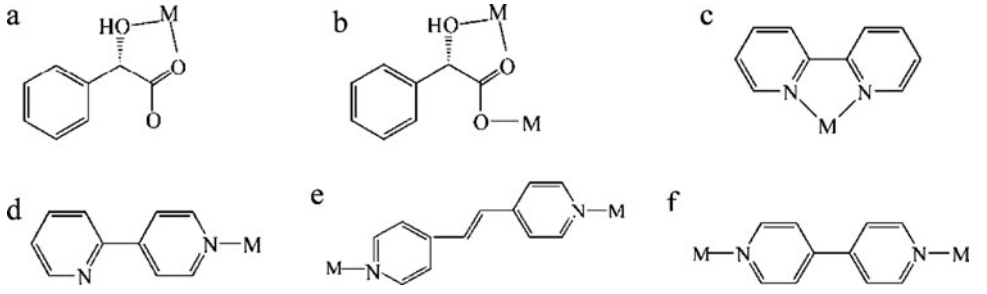

Scheme 1. (a) The observed coordination modes of H_2mand for **1**, **2**, **3** and **4**. (b) The observed coordination modes of H_2mand for **5** and **6.** (c) The observed coordination modes of 2,2′-bipy for **1** and **2**. (d) The observed coordination modes of 2,4′-bipy for **4**. (e) The observed coordination modes of bpe for **3** and **5**. (f) The observed coordination modes of 4,4′-bipy for **6**.

Table 3. Hydrogen bond lengths (Å) and angles (°) for **1**.

D–H···A	d(D–H)	d(H···A)	d(D···A)	<(DHA)
O(4)–H(4A)···O(1)#2	0.85	2.08	2.880(9)	157.8
O(3)–H(3)···O(1)#3	0.81	1.73	2.543(8)	171.5

Notes: Symmetry transformations used to generate equivalent atoms: #1 x, $x-y$, $-z+1/6$; #2 $x-y+1$, $-y+1$, $-z$; #3 $x-y$, x, $z+1/6$.

in an adjacent chain with O3…O1 distances 2.543(8) Å, as shown in figure 1(b). These units are connected by hydrogen bond interactions among $Hmand^-$ and H_2O, giving a 1-D supramolecular arrangement.

The single-crystal X-ray diffraction studies reveal that **2** adopts a structure very similar to that of **1** (figure S1(a)–(b)), as shown by the detailed structural data listed in the Supplementary material. Moreover, the Ni–O bond lengths range from 2.050(3) to 2.072(3) Å and the Ni–N bond length is 2.060(5) Å. The intermolecular hydrogen bonding data listed in table 4.

3.1.2. Structure of $[Ni(Hmand)_2(bpe)]_n$ (3). The single-crystal X-ray diffraction analysis reveals that **3** crystallizes in the monoclinic space group *C*2/c and features a 1-D infinite chain. The asymmetric unit of **3** contains one Ni^{2+}, two $Hmand^-$ anions, and one bpe ligand, as shown in figure 2(a). The geometry around Ni^{2+} is octahedral. In the equatorial plane, each Ni^{2+} is surrounded by two $Hmand^-$ ligands, each chelating the metal through one oxygen of the carboxylate group (O1) and the hydroxyl oxygen (O3). Two nitrogens (N1, $N1^{\#2}$) from two different bpe molecules occupy the axial positions. Surprisingly, the

Table 4. Hydrogen bond lengths (Å) and angles (°) for **2**.

D–H···A	d(D–H)	d(H···A)	d(D···A)	<(DHA)
O(4)–H(4A)···O(3)#2	0.91	2.16	2.941(6)	143.3
O(1)–H(1A)···O(3)#3	0.91	1.64	2.547(4)	173.7

Notes: Symmetry transformations used to generate equivalent atoms: #1 x, $x-y+2$, $-z+1/6$; #2 y, $-x+y$, $z-1/6$; #3 $y-1$, $-x+y$, $z-1/6$.

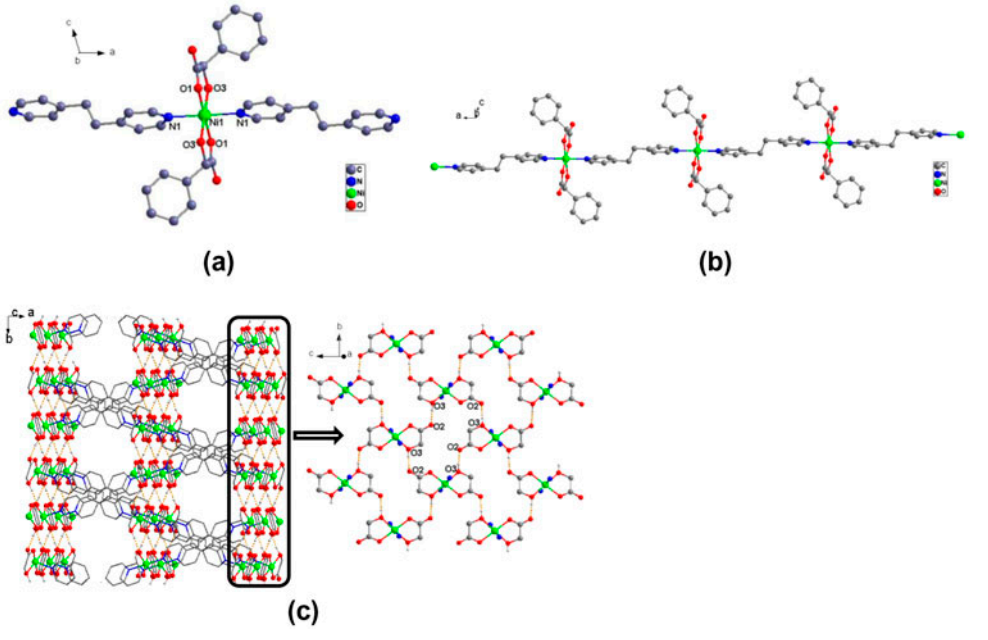

Figure 2. X-ray crystal structure of **3**. (a) The coordination environment of the Ni center for **3** (hydrogens have been omitted for clarity). (b) The 1-D chain structure for **3** (hydrogens have been omitted for clarity). (c) A view of the supramolecular 3-D network of **3**.

bond angles of $N1^{\#2}$–Ni1–N1, O1–Ni1–$O1^{\#2}$ and O3–Ni1–$O3^{\#2}$ are 180.0°, respectively. In this complex, the coordination polyhedra are distorted octahedral with the main deviations from regularity affecting the chelating angles $O_{hydroxyl}$–Ni–$O_{carboxy}$ (O1–Ni1–O3 = 80.57 (4)°). The Ni–O bond lengths are 2.0103(10)–2.0624(10) Å and the Ni–N bond length is 2.1343(13) Å.

Each $Hmand^-$ is a bidentate chelate ligand (scheme 1(a)). Each bpe is a bidentate bridging ligand to connect two Ni(II) cations to form a 1-D infinite chain (scheme 1(e)), as shown in figure 2(b). Adjacent chains are connected via hydrogen bonding between uncoordinated carboxylato oxygen (O2) and hydroxyl oxygen (O3) of $Hmand^-$ (O3–H3A···$O2^{\#3}$ = 2.5777(14) Å) (listed in table 5). Four discrete nickel units are involved in forming a puckered 18-membered ring. Every puckered 18-membered ring consolidates four 1-D chains by hydrogen bonding and further extends it into a 3-D supramolecular structure, as shown in figure 2(c).

Table 5. Hydrogen bond lengths (Å) and angles (°) for **3**.

D–H···A	d(D–H)	d(H···A)	d(D···A)	<(DHA)
O(3)–H(3A)···O(2)#3	0.9	1.68	2.577(14)	173.1

Notes: Symmetry transformations used to generate equivalent atoms: #1 $-x+1, -y, -z+2$; #2 $-x+1/2, -y+1/2, -z+2$; #3 $-x+1/2, y-1/2, -z+3/2$.

3.1.3. Structure of $[Zn(Hmand)_2(2,4'\text{-bipy})(H_2O)]\cdot 2H_2O$ (4). Single-crystal X-ray diffraction analysis reveals that **4** comprises discrete molecular units which crystallize in the monoclinic space group $P2_1$. In **4,** the asymmetric unit is composed of one Zn^{2+}, two $Hmand^-$ ligands, one 2,4′-bipy group, one coordinated water, and two lattice waters, as shown in figure 3(a). The Zn^{2+} of **4** is six-coordinate in a distorted octahedral coordination sphere by N1 that is derived from one 2,4′-bipy group, O7 originating from the coordinated water, and O2, O3, O4, and O6 from the carboxyl and hydroxyl groups of two different $Hmand^-$ ligands, respectively. The O2, O4, O6, and O7 form the equatorial plane, while N1 and O3 are located in the axial positions. The Zn–O bond lengths are 2.0649(14)–2.1248(17) Å. The Zn–N bond length is 2.119(2) Å.

The $Hmand^-$ is a monoanionic O,O′-bidentate ligand that chelates Zn^{2+} through carboxylic and hydroxyl oxygens to form a five-membered chelate ring (scheme 1(a)). Moreover, 2,4′-bipy is only a monodentate ligand (scheme 1(d)). Many strong intermolecular hydrogen bonds can be found in this coordination compound. The nine intermolecular hydrogen bonds (listed in table 6) between two lattice water molecules, a coordinated water molecule, carboxylic and the hydroxyl oxygens lead to the assembly of these monomeric units forming a 2-D supramolecular structure, as shown in figure 3(b). In addition, the 2-D sheets in **4** are linked by the offset $\pi\cdots\pi$ stacking interaction (3.4887 Å) between the $Hmand^-$ and 2,4′-bipy linkers to form a supramolecular 3-D network, as shown in figure 3(c).

3.1.4. Structure of $[Zn(Hmand)(bpe)(H_2O)]_n[(ClO_4)]_n\cdot nH_2O$ (5). Single-crystal X-ray diffraction analysis reveals that **5** presents a 2-D structure which crystallizes in the monoclinic space group $P2_1$. In **5,** the asymmetric unit is composed of $[Zn(Hmand)(bpe)(H_2O)]^+$

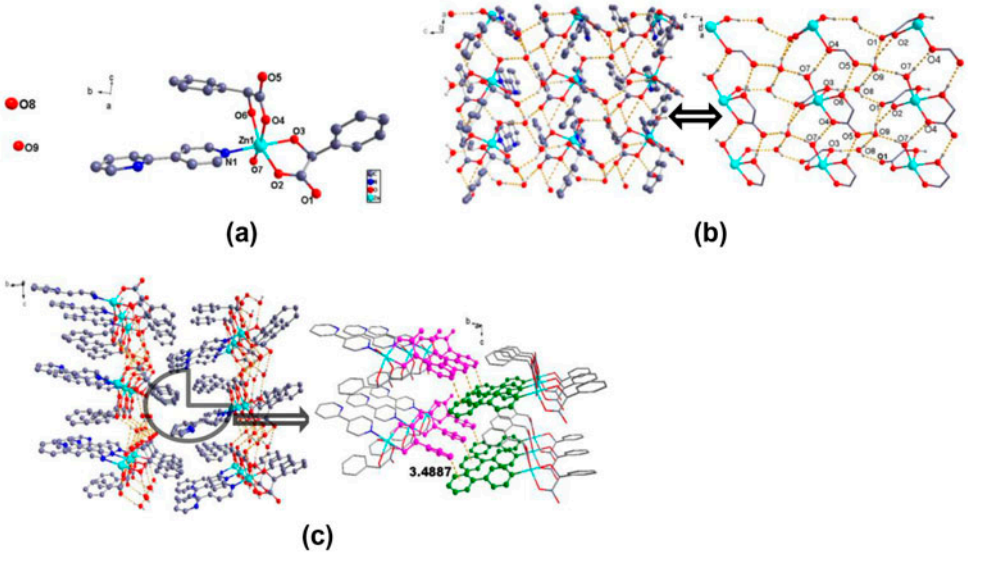

Figure 3. X-ray crystal structure of **4**. (a) The coordination environment of the Zn center for **4** (hydrogens have been omitted for clarity). (b) The 2-D supramolecular architecture through hydrogen-bonding interactions for **4**. (c) The $\pi\cdots\pi$ interactions linking **4** into a 3-D supramolecular structure.

Table 6. Hydrogen bond lengths (Å) and angles (°) for **4**.

D–H···A	d(D–H)	d(H···A)	d(D···A)	<(DHA)
O(9)–H(9B)···O(5)#1	0.85	1.95	2.773(3)	162.5
O(9)–H(9A)···O(2)#2	0.85	2.50	3.048(2)	123.3
O(9)–H(9A)···O(1)#2	0.85	1.90	2.731(3)	163.8
O(8)–H(8B)···O(9)#3	0.85	1.89	2.732(3)	170.9
O(8)–H(8A)···O(1)#2	0.85	2.03	2.808(3)	151.5
O(7)–H(7B)···O(9)#4	0.85	1.90	2.742(3)	170.6
O(7)–H(7A)···O(4)#5	0.85	1.94	2.724(2)	152.5
O(6)–H(6)···O(5)#5	0.81	1.85	2.659(2)	172.2
O(3)–H(3A)···O(8)#6	0.91	1.67	2.576(3)	173.8

Notes: Symmetry transformations used to generate equivalent atoms: #1 $-x+1, y+1/2, -z+1$; #2 $-x+1, y+1/2, -z$; #3 $x-1, y, z$; #4 $-x+2, y-1/2, -z$; #5 $x+1, y, z$; #6 $-x+1, y-1/2, -z+1$.

and, in the outer coordination sphere, ClO_4^-, and one lattice water, as depicted in figure 4(a). Each zinc ion is six-coordinate, with a slightly distorted octahedral geometry. The coordination sphere consists of four oxygens (O1, O2, O3) from two $Hmand^-$ and one water (O4), and N1 and N2 from two different bpe ligands. Two nitrogens are in axial positions and four oxygens are in equatorial positions. The Zn–O bond lengths are 2.124 (5)–2.274(4) Å. The Zn–N bond lengths are 2.099(4) Å and 2.113(4) Å.

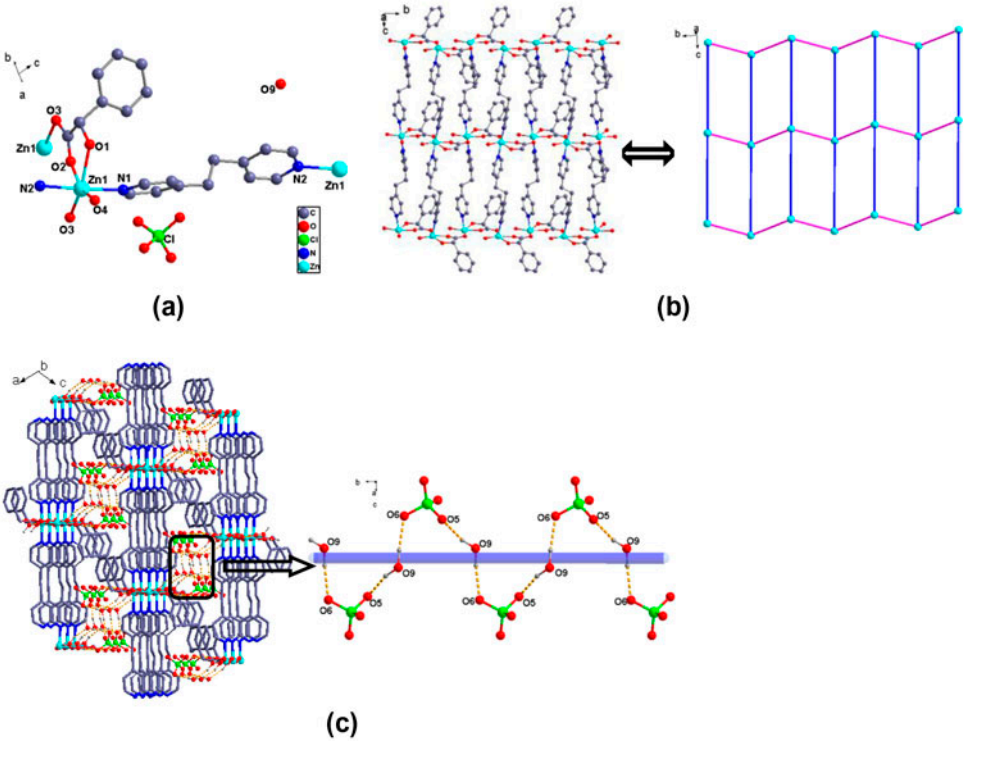

Figure 4. X-ray crystal structure of **5**. (a) The coordination environment of the Zn center for **5** (hydrogens have been omitted for clarity). (b) View of 2-D structure of **5**. (c) Representation of the 3-D supramolecular network connected through hydrogen bonds of **5** and supramolecular left-handed helical chain.

Table 7. Hydrogen bond lengths (Å) and angles (°) for **5**.

D–H···A	d(D–H)	d(H···A)	d(D···A)	<(DHA)
O(4)–H(4A)···O(3)#5	0.82	2.01	2.816(8)	169.0
O(4)–H(4A)···O(2)#4	0.82	2.47	2.924(5)	116.0
O(4)–H(4B)···O(9)#6	0.91	1.91	2.790(6)	161.2
O(9)–H(9A)···O(5)#7	0.97	2.01	2.956(7)	164.9
O(9)–H(9B)···O(6)#8	0.98	2.06	3.036(6)	170.4

Notes: Symmetry transformations used to generate equivalent atoms: #1 $x + 1$, y, $z + 1$; #2 $-x$, $y + 1/2$, $-z$; #3 $x - 1$, y, $z - 1$; #4 $-x$, $y - 1/2$, $-z$; #5 x, $y - 1$, z; #6 $-x$, $y - 1/2$, $-z + 1$; #7 $-x + 1$, $y + 1/2$, $-z + 1$; #8 x, y, $z + 1$.

In **5**, $Hmand^-$ are chelating-bridging tridentate ligands through their hydroxyl and carboxylate groups toward the two Zn^{2+} cations (scheme 1(b)), involving three oxygens (that is, a pair of carboxylic oxygens from the carboxyl group and one oxygen from the hydroxyl group). Extension of the structure through the bridging $Hmand^-$ ligand generates a zigzag chain with a Zn–Zn distance of 4.6951(10) Å inside the chain. Adjacent chains are interconnected via the tethering bpe ligands to generate a chiral layer (scheme 1(e)), as shown in figure 4(b). The cationic $[Zn(Hmand)(bpe)(H_2O)]_n^+$ layers require additional counter anions to maintain the overall charge balance. The required uncoordinated ClO_4^- anions are readily accommodated between the double-layer motifs.

Significantly, the uncoordinated ClO_4^- anions are involved in hydrogen bonding with the lattice water molecules (O9–H9A···$O5^{\#7}$ = 2.956(7) Å, O9–H9B···$O6^{\#8}$ = 3.036(6) Å). The propagation of these hydrogen bonds leads to the construction of a 1-D hydrogen-bonded supramolecular left-handed helical chain. The adjacent layers are linked to each other via O–H···O (listed in table 7) interactions between the supramolecular left-handed helical chain and adjacent coordinated oxygens to lead to a 3-D supramolecular structure viewed along the *b* axis, as shown in figure 4(c).

3.1.5. Structure of $[Zn(Hmand)(4,4'\text{-bipy})(H_2O)]_n[(ClO_4)]_n$ (6). Single-crystal X-ray diffraction indicates that **6** crystallizes in the monoclinic space group $P2_1$. Each crystallographic unit consists of one Zn^{2+}, one $Hmand^-$, one 4,4′-bipy molecule, one coordinated water, and one perchlorate. The coordination sphere is similar to that for **5** except that bpe was replaced by 4,4′-bipy, as shown in figure 5(a); each Zn^{2+} has octahedral coordination geometry, surrounded by two nitrogens (N1 and N2) and four oxygens (O1, O2, O3, and O8). O1, O2, O3, and O8 form the equatorial plane, while N1 and N2 are in axial positions. The Zn–O and Zn–N bond lengths are 2.098(3)–2.228(3) Å and 2.131(3)–2.135(3) Å, respectively.

$Hmand^-$ uses a chelating-bridging tridentate mode to connect two Zn^{2+} cations with a pair of carboxylic oxygens and hydroxyl oxygen (scheme 1(b)). All of the Zn centers are bridged by $Hmand^-$ ligands to form a 1-D zigzag chain that extends along the b-direction. These 1-D chains are further connected by the 4,4′-bipy ligands to form a 2-D layer parallel to the *bc* plane (scheme 1(f)), with shortest Zn···Zn separations between adjacent chains of 11.35 Å, as shown in figure 5(b). The 2-D layers are further connected and stabilized by hydrogen-bonding interactions (O8–H8A···$O7^{\#3}$ = 2.882(4), O3–H3A···$O5^{\#3}$ = 2.729(4), O8–H8B···$O1^{\#5}$ = 2.764(5)) (listed in table 8), as shown in figure 5(c).

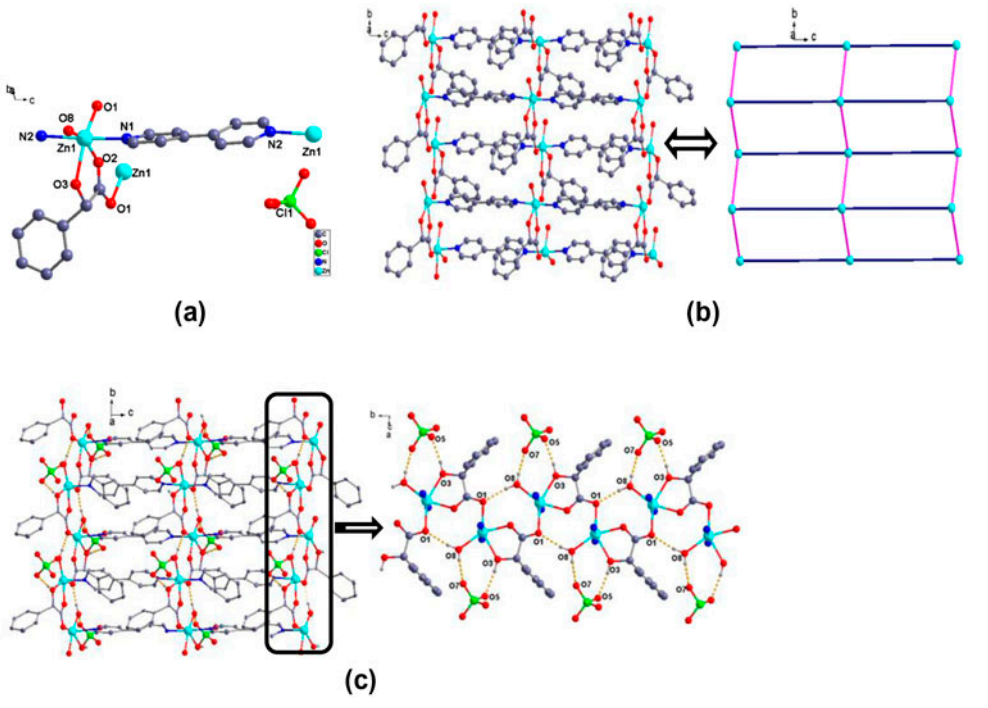

Figure 5. X-ray crystal structure of **6**. (a) The coordination environment of the Zn center for **6** (hydrogens have been omitted for clarity). (b) View of 2-D structure of **6**. (c) The 2-D supramolecular architecture through hydrogen-bonding interactions of **6**.

Table 8. Hydrogen bond lengths (Å) and angles (°) for **6**.

D–H···A	d(D–H)	d(H···A)	d(D···A)	<(DHA)
O(8)–H(8A)···O(7)#3	0.85	2.03	2.882(4)	175.0
O(3)–H(3A)···O(5)#3	0.84	1.90	2.729(4)	167.8
O(8)–H(8B)···O(1)#5	0.85	1.93	2.764(5)	166.0

Notes: Symmetry transformations used to generate equivalent atoms: #1 x, y, $z+1$; #2 $-x+2$, $y-1/2$, $-z$; #3 x, y, $z-1$; #4 $-x+2$, $y+1/2$, $-z$; #5 x, $y+1$, z.

3.2. *Comparative analysis of the structures of these compounds*

From the structure descriptions above, the coordination mode of the auxiliary ligands affects the structural features of **1**–**6**. In this work, we select four N-donor ligands (2,2′-bipy, 2,4′-bipy, 4,4′-bipy, and bpe) to observe their effect on the assembly of the coordination compounds. In **3**, **5,** and **6**, bpe and 4,4′-bipy are bidentate bridging, promoting the formation of higher dimensional complexes. The introduction of the chelating ligands 2,2′-bipy and 2,4′-bipy generally result in drastic change of the structures. For instance, in **5**, the bpe ligands bridge Zn^{2+} cations in a 1-D chain. However, when 2,4′-bipy is introduced into the reaction system of **5**, a 0-D structure **4** is obtained. The formation of the low dimensional structure of **1**(**2**) may be attributable to the steric hindrance of the chelating 2,2′-bipy ligand. From

the results above, we can see that the N-donor ligands play an important role in the formation of the final complex structures.

Compounds 4, **5,** and **6** with the same metal ion have the same coordination numbers and reaction conditions. However, significant differences are found in the final frameworks. Mandelic acid displays two different coordination modes in **4**, **5,** and **6**. In **4**, $Hmand^-$ links one M(II) in bidentate-chelate coordination. In **5** and **6**, each $Hmand^-$ connects two metal cations in a chelating-bridging tridentate coordination mode and form a 1-D infinite chain. X-ray analyses reveal that the versatility of this ligand upon coordination to a zinc(II) may be influenced by the counter anions. Additionally, hydrogen-bonding interactions and π–π stacking interactions contribute to the formation of the diverse supramolecular architectures. Further comparative analysis of some reported chiral structures which utilize chiral ligands and N-donor ligands in different conditions [32–34] show intriguing 1-D, 2-D, and 3-D structures, and the chiral ligands act as diverse linkers connecting metal cations. Then the N-donor ligand with different lengths are employed to enrich the versatility of the structures and gain a deeper insight into the influence of ligand length on the compounds' structures. Comparing complexes we observe that ligand and N-donor ligand play a crucial role in the structural diversity.

3.3. *Infrared spectra and thermogravimetric analysis*

The strong and broad absorptions at 3308–3524 cm^{-1} indicate the presence of ν_{as}(O–H) of H_2mand. The ν_{as}(COO–) and ν_s(COO–) vibrations can be observed at 1578–1585 and 1373–1450 cm^{-1}, respectively. The characteristic IR band of 2,2′-bipy at 1475 cm^{-1} is due to $\nu_{C=N}$ vibrations for **1** and **2**. The IR band of bpe at 1378–1429 and 1612–1616 cm^{-1} is due to $\nu_{C=C}$ and $\nu_{C=N}$ vibrations for **3** and **5**. 2,4′-bipy shows stretches at 1419 and 777 cm^{-1} for **4**. Compound **6** shows $\nu_{C=C}$ and $\nu_{C=N}$ stretches of 4,4′-bipy at 1611 and 1412 cm^{-1}, respectively.

Thermogravimetric experiments were performed on solid samples consisting of numerous single crystals from 20 to 800 °C under N_2. According to the TGA curves, **1** and **2** display similar thermal decomposition behavior. The first weight loss from 30 to 181 °C corresponds to release of one lattice water per formula unit (Obsd, 2.74%, 3.69%; Calcd, 3.36%, 3.36%, respectively). Further weight losses from 181 to 600 °C could be attributed to decomposition of the framework to form CoO/NiO as the final product (Obsd, 14.74%, 12.86%; Calcd, 13.99%, 13.95%, respectively). Compound **3** has no obvious weight loss before 297 °C, which is consistent with the absence of solvent in the crystal structure. Then the framework collapses with an abrupt weight loss as a result of ligand decomposition. The remaining weight corresponds to NiO as the residue (Obsd 14.01%, Calcd 13.70%). For **4**, the preliminary weight loss from 105 to 153 °C is consistent with removal of three lattice waters (Obsd 9.84%, Calcd 9.34%). The second weight loss corresponds to expulsion of bipy from 153 to 269 °C (Obsd, 27.38% and Calcd, 27.03%). The TGA curve of **5** exhibits an initial weight loss from room temperature to 114 °C, with the observed weight loss of 3.77% (Calcd 3.36%) corresponding to the escape of one lattice water molecule. Compound **5** continues to lose weight up to 800 °C, indicating the continuous expulsion of organic moieties even at the upper limit of the measurement range. The TGA curve of **6** shows a weight loss at 102–168 °C attributed to the loss of a half-coordinated water (Obsd 1.84%, Calcd 1.85%). Two weight-loss processes from 168 to 258 °C and 258 to 785 °C indicate that the complex completely decomposes. The final mass remnant is roughly consistent with a deposition of ZnO (Obsd 16.61%, Calcd 19.58%) (Supporting information, figure S3).

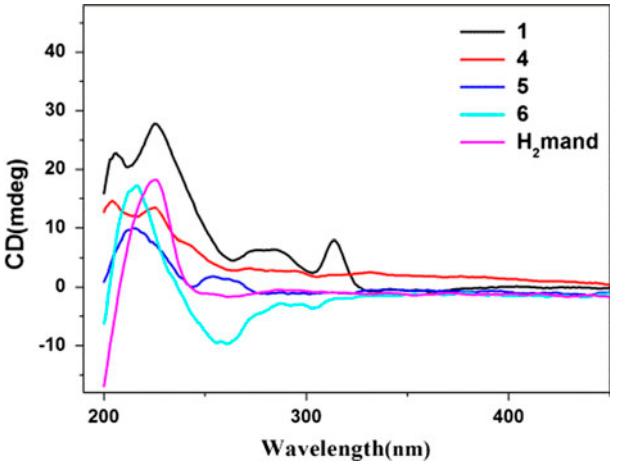

Figure 6. The solid-state CD spectra of bulk samples of H_2mand and **1**, **4**, **5** and **6**.

3.4. *PXRD and solid-state CD spectra*

To check the phase purity of the products, PXRD experiments were recorded for **1**–**6** at room temperature. The main peaks of simulated spectra of **1**–**6** are basically consistent with their experimental spectra, demonstrating that the bulk synthesized materials and the measured single crystals are the same. The differences in intensity may be attributed to the preferred orientation of the crystal samples (Supporting information, figure S4).

To further examine the chiroptical activities, the solid-state CD spectra of H_2mand and **1**, **4**, **5,** and **6** were measured in KCl pellet, as shown in figure 6. Chiral H_2mand exhibits one positive peak around 225 nm. Bulk samples of **1**, **4**, **5,** and **6** displayed approximate curves in the region of 204–250 nm, showing that they all have the chiral conformation. The formation of the chiral structures of **1**, **4**, **5,** and **6** have influence on the direction (+ or −) of the CD signals except for a slight shift of the absorption peaks position compared with H_2mand. This indicates the CD chromophore mostly comes from the ligand H_2mand and confirms that the entire crystal products of **1**, **4**, **5,** and **6** are homochiral.

3.5. *Photoluminescent property*

Coordination compounds, especially those with d^{10} metal centers, are investigated for their fluorescent properties and potential applications. Therefore, the photoluminescence properties of **4**–**6** and free ligands were measured in the solid state, as shown in figure 7.

The free ligands emit strong fluorescence centered at 572 nm (λ_{ex} = 240 nm) for H_2mand, 444 nm (λ_{ex} = 370 nm) for 4,4′-bipy, and 364 nm (λ_{ex} = 300 nm) for bpe; there is no obvious emission observed for free 2,4′-bipy under the same experimental conditions. The fluorescence of these ligands may be assigned to $\pi^* \rightarrow n$ and $\pi^* \rightarrow \pi$ transitions of the intraligands [35–37]. Maximum emissions are observed at *ca.* 532 nm for **4** (λ_{ex} = 348 nm), 698 nm for **5** (λ_{ex} = 285 nm), and 371 nm for **6** (λ_{ex} = 328 nm), respectively. In comparison with those of free 4,4′-bipy, the emission peak for **6** may originate from intraligand emission of 4,4′-bipy because the fluorescent emission bands are similar to that of the ligands.

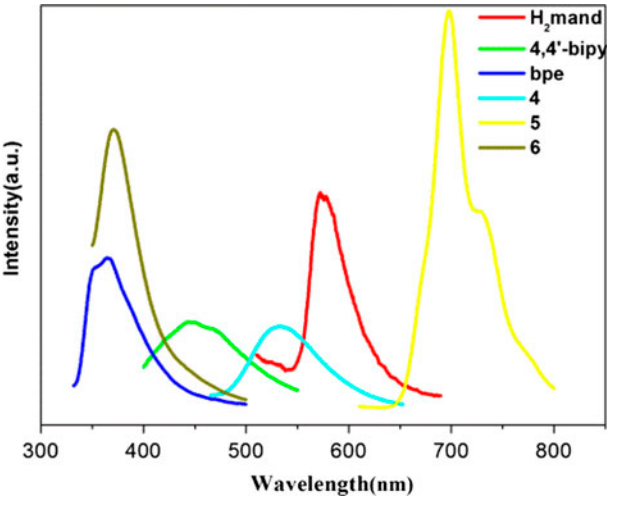

Figure 7. Emission spectra of **4**, **5**, **6**, H_2mand, 4,4′-bipy and bpe.

Similar to **6**, compound **4** can be tentatively assigned to intraligand fluorescence since the free ligand exhibited a similar emission under the same condition [38, 39]. However, the emission of **5** occurs at quite a low energy of 698 nm with large Stokes shift, which can be assigned to a ligand-to-metal charge transfer transition [40, 41]. The blue or red shifts of emission occurring in **4**–**6** are assigned to different coordination environments around the metal ions, a phenomenon which also appears in other compounds [42–44].

4. Conclusion

Seven compounds using (*S*)-(+)-mandelic acid have been synthesized and structurally characterized. Compounds **1**–**6** show 0-D, 1-D, and 2-D structures. Compounds **1**, **2,** and **4** have 0-D structures, **3** exhibits 1-D chain structure, **5** and **6** have 2-D undulated networks. Many strong intermolecular hydrogen bonds are found in **1**–**6**, which contribute to the formation of the diverse supramolecular architectures. The structural diversities of the complexes demonstrate that H_2mand creates many possibilities to synthesize coordination compounds with intriguing structures and shows that N-donor ligands play roles in the formation of the complexes. Compounds **1**, **2**, **4**, **5,** and **6** crystallize in chiral space groups and their CD spectra exhibit positive cotton effects. Compound **3** possesses the centrosymmetric space group of *C*2/c as a result of racemization of the H_2mand due to the severe reaction conditions [17, 22]. The luminescent properties of **4**–**6** were examined in solid states at room temperature. The emission discrepancy of these compounds is closely associated to the differences of the N-donor ligands and the H_2mand coordinated around the Zn ions.

Disclosure statement

No potential conflict of interest was reported by the authors.

Funding

This work was supported by the Natural Science Foundation of China [grant number 21141002], [grant number 21272054], [grant number 21072043]; the Natural Science Foundation of Hebei Province [grant number B2012205040], [grant number B201000362]; and Doctoral Foundation of Hebei Normal University [grant number 130374].

Supplemental data

Supplemental data for this article can be accessed http://dx.doi.org/10.1080/00958972.2015.1100300.

References

[1] T. Kaczorowski, I. Justyniak, T. Lipińska, J. Lipkowski, J. Lewiński. *J. Am. Chem. Soc.*, **131**, 5393 (2009).
[2] G. Shemer, O. Krichevski, G. Markovich, T. Molotsky, I. Lubitz, A.B. Kotlyar. *J. Am. Chem. Soc.*, **133**, 1278 (2011).
[3] C.M. Liu, R.G. Xiong, D.Q. Zhang, D.B. Zhu. *J. Am. Chem. Soc.*, **132**, 4044 (2010).
[4] S. Banerjee, N.N. Adarsh, P. Dastidar. *CrystEngComm*, **11**, 746 (2009).
[5] L. Lin, R. Yu, W. Yang, X.-Y. Wu, C.-Z. Lu. *Cryst. Growth Des.*, **12**, 3304 (2012).
[6] (a) G. Li, W.B. Yu, J. Ni, T.F. Liu, Y. Liu, E.H. Sheng, Y. Cui. *Angew. Chem.*, **120**, 1265 (2008); (b) Y. Liu, W.M. Xuan, Y. Cui. *Adv. Mater.*, **22**, 4112 (2010); (c) C. Zhu, G. Yuan, X. Chen, Z. Yang, Y. Cui. *J. Am. Chem. Soc.*, **134**, 8058 (2012).
[7] S.-F. Zhu, B. Xu, G.-P. Wang, Q.-L. Zhou. *J. Am. Chem. Soc.*, **134**, 436 (2012).
[8] T. Hang, D.W. Fu, Q. Ye, R.G. Xiong. *Cryst. Growth Des.*, **9**, 2026 (2009).
[9] Z.-G. Gu, Y.-F. Xu, X.-J. Yin, X.-H. Zhou, J.-L. Zuo, X.-Z. You. *Dalton Trans.*, **41**, 5593 (2008).
[10] L. Croitor, E.B. Coropceanu, A.V. Siminel, V.Ch. Kravtsov, M.S. Fonari. *Cryst. Growth Des.*, **11**, 3536 (2011).
[11] A. Mallick, S. Saha, P. Pachfule, S. Roy, R. Banerjee. *J. Mater. Chem.*, **20**, 9073 (2010).
[12] Z. Su, M.S. Chen, J. Fan, M. Chen, S.S. Chen, L. Luo, W.Y. Sun. *CrystEngComm*, **12**, 2040 (2010).
[13] M.L. Li, H.H. Song. *J. Solid State Chem.*, **206**, 182 (2013).
[14] F. Li, T.H. Li, X.J. Li, X. Li, Y.L. Wang, R. Cao. *Cryst. Growth Des.*, **6**, 1458 (2006).
[15] T. Shiga, M. Takeo, F. Iijima, G.N. Newton, H. Oshio. *New J. Chem.*, **38**, 1946 (2014).
[16] Y. Zhang, J. Yang, Y. Yang, J. Guo, J.F. Ma. *Cryst. Growth Des.*, **12**, 4060 (2012).
[17] R. He, H.-H. Song, Z. Wei, J.-J. Zhang, Y.-Z. Gao. *J. Solid State Chem.*, **183**, 2021 (2010).
[18] W. Huang, Y. Jin, D. Wu, G. Wu. *Inorg. Chem.*, **53**, 73 (2014).
[19] S.S. Sunkari, B. Kharediya, S. Saha, B. Elrez, J.P. Sutter. *New J. Chem.*, **38**, 3529 (2014).
[20] C. Shen, T. Sheng, C. Tian, Q. Zhu, X. Wu. *Inorg. Chem. Commun.*, **17**, 142 (2012).
[21] E. Bermejo, R. Carballo, A. Castiñeiras, A.B. Lago. *Coord. Chem. Rev.*, **257**, 2639 (2013).
[22] M. Moriya, S. Tominaga, T. Hashimoto, K. Tanifuji, T. Matsumoto, Y. Ohki, K. Tatsumi, J. Kaneshiro, Y. Uesu, W. Sakamoto, T. Yogo. *Inorg. Chem.*, **51**, 4689 (2012).
[23] P. Halder, E. Zangrando, T.K. Paine. *Polyhedron*, **29**, 434 (2010).
[24] R. Carballo, A. Castiñeiras, S. Balboa, B. Covelo, J. Niclós. *Polyhedron*, **21**, 2811 (2002).
[25] R. Carballo, B. Covelo, E.M. Vázquez-López, E. García-Martínez, A. Castiñeiras, J. Niclós. *Z. Anorg. Allg. Chem.*, **631**, 785 (2005).
[26] D.N. Dybtsev, M.P. Yutkin, D.G. Samsonenko, V.P. Fedin, A.L. Nuzhdin, A.A. Bezrukov, K.P. Bryliakov, E.P. Talsi, R.V. Belosludov, H. Mizuseki, Y. Kawazoe, O.S. Subbotin, V.R. Belosludov. *Chem. Eur. J.*, **16**, 10348 (2010).
[27] G. Novitchi, G. Pilet, D. Luneau. *Eur. J. Inorg. Chem.*, **2011**, 4869 (2011).
[28] L.L. Wu, H.H. Song, R. He, H.T. Yu. *Inorg. Chim. Acta*, **399**, 6 (2013).
[29] R. He, H. Song, Z. Wei. *Inorg. Chim. Acta*, **363**, 2631 (2010).
[30] Q. Feng, M. Yan, L. Wu, H. Song, H. Yu. *Inorg. Chem. Commun.*, **43**, 1 (2014).
[31] G. Zhang, X. Zhou, T. Li, X. Meng. *Inorg. Chim. Acta*, **421**, 45 (2014).
[32] J.-L. Qi, S.-L. Ni, W. Xu, Y.-Q. Zheng. *J. Coord. Chem.*, **67**, 2287 (2014).
[33] H.-T. Ye, C.-Y. Ren, G.-F. Hou, Y.-H. Yu, X. Xu, J.-S. Gao, P.-F. Yan, S.-W. Ng. *Cryst. Growth Des.*, **14**, 3309 (2014).
[34] Y. Wen, T. Sheng, Z. Xue, Z. Sun, Y. Wang, S. Hu, Y. Huang, J. Li, X. Wu. *Cryst. Growth Des.*, **14**, 6230 (2014).
[35] L.P. Zhang, J.F. Ma, J. Yang, Y.Y. Liu, G.H. Wei. *Cryst. Growth Des.*, **9**, 4661 (2009).

[36] J.K. Nath, A. Mondal, A.K. Powell, J.B. Baruah. *Cryst. Growth Des.*, **14**, 4735 (2014).
[37] D. Niu, J. Yang, J. Guo, W.-Q. Kan, S.-Y. Song, P. Du, J.-F. Ma. *Cryst. Growth Des.*, **12**, 2397 (2012).
[38] J. Liu, H.B. Zhang, Y.X. Tan, F. Wang, Y. Kang. *Inorg. Chem.*, **53**, 1500 (2014).
[39] Y.-Y. Liu, Y.-Y. Jiang, J. Yang, Y.-Y. Liu, J.-F. Ma. *CrystEngComm*, **13**, 6118 (2011).
[40] S.-S. Chen, Q. Liu, Y. Zhao, R. Qiao, L.-Q. Sheng, Z.-D. Liu, S. Yang, C.-F. Song. *Cryst. Growth Des.*, **14**, 3727 (2014).
[41] Y.L. Wang, Q.Y. Liu, L. Xu. *CrystEngComm.*, **10**, 1667 (2008).
[42] J.-Y. Wu, P.-T. Yuan, C.-C. Hsiao. *CrystEngComm*, **16**, 3128 (2014).
[43] L. Cheng, J. Wang, H.-Y. Yu, X.-Y. Zhang, S.-H. Gou, L. Fang. *J. Solid State Chem.*, **221**, 85 (2015).
[44] L.-H. Cao, Y.-L. Wei, Y. Yang, H. Xu, S.-Q. Zang, H.-W. Hou, T.C.W. Mak. *Cryst. Growth Des.*, **14**, 1827 (2014).